



Long-term real-time measurements of aerosol particle composition in Beijing, China: seasonal variations, meteorological effects, and source analysis

Y. L. Sun¹, Z. F. Wang¹, W. Du^{1,2}, Q. Zhang³, Q. Q. Wang¹, P. Q. Fu¹, X. L. Pan⁴, J. Li¹, J. Jayne⁵, and D. R. Worsnop⁵

¹State Key Laboratory of Atmospheric Boundary Layer Physics and Atmospheric Chemistry, Institute of Atmospheric Physics, Chinese Academy of Sciences, Beijing 100029, China

²Department of Resources and Environment, Air Environmental Modeling and Pollution Controlling Key Laboratory of Sichuan Higher Education Institutes, Chengdu University of Information Technology, Chengdu 610225, China

³Department of Environmental Toxicology, University of California, 1 Shields Ave., Davis, CA 95616, USA

⁴Research Institute for Applied Mechanics, Kyushu University, Fukuoka, Japan

⁵Aerodyne Research, Inc., Billerica, MA 01821, USA

Correspondence to: Y. L. Sun (sunyele@mail.iap.ac.cn)

Received: 14 April 2015 – Published in Atmos. Chem. Phys. Discuss.: 22 May 2015

Revised: 31 August 2015 – Accepted: 1 September 2015 – Published: 11 September 2015

Abstract. High concentrations of fine particles (PM_{2.5}) are frequently observed during all seasons in Beijing, China, leading to severe air pollution and human health problems in this megacity. In this study, we conducted real-time measurements of non-refractory submicron aerosol (NR-PM₁) species (sulfate, nitrate, ammonium, chloride, and organics) in Beijing using an Aerodyne Aerosol Chemical Speciation Monitor for 1 year, from July 2011 to June 2012. This is the first long-term, highly time-resolved (~15 min) measurement of fine particle composition in China. The seasonal average ($\pm 1\sigma$) mass concentration of NR-PM₁ ranged from 52 (± 49) $\mu\text{g m}^{-3}$ in the spring season to 62 (± 49) $\mu\text{g m}^{-3}$ in the summer season, with organics being the major fraction (40–51%), followed by nitrate (17–25%) and sulfate (12–17%). Organics and chloride showed pronounced seasonal variations, with much higher concentrations in winter than in the other seasons, due to enhanced coal combustion emissions. Although the seasonal variations of secondary inorganic aerosol (SIA, i.e., sulfate + nitrate + ammonium) concentrations were not significant, higher contributions of SIA were observed in summer (57–61%) than in winter (43–46%), indicating that secondary aerosol production is a more important process than primary emissions in summer. Organics presented pronounced diurnal cycles that were similar among all seasons, whereas the diurnal variations of nitrate

were mainly due to the competition between photochemical production and gas–particle partitioning. Our data also indicate that high concentrations of NR-PM₁ ($> 60 \mu\text{g m}^{-3}$) are usually associated with high ambient relative humidity (RH) ($> 50\%$) and that severe particulate pollution is characterized by different aerosol composition in different seasons. All NR-PM₁ species showed evident concentration gradients as a function of wind direction, generally with higher values associated with wind from the south, southeast or east. This was consistent with their higher potential as source areas, as determined by potential source contribution function analysis. A common high potential source area, located to the southwest of Beijing along the Taihang Mountains, was observed during all seasons except winter, when smaller source areas were found. These results demonstrate a high potential impact of regional transport from surrounding regions on the formation of severe haze pollution in Beijing.

1 Introduction

Severe haze pollution episodes, characterized by high concentrations of fine particles (PM_{2.5}), occur frequently during all seasons in China (Sun et al., 2013b; Guo et al., 2014; Zheng et al., 2015), not only reducing visibility sig-

nificantly, but also exerting harmful effects on public health (Cao et al., 2012). The mass concentrations of $\text{PM}_{2.5}$ often far exceed the China National Ambient Air Quality Standard (NAAQS; $75 \mu\text{g m}^{-3}$ as a 24 h average), particularly in the economically developed regions of Beijing–Tianjin–Hebei and Yangtze River Delta (YRD). According to Beijing Environmental Statements, the annual average mass concentration of $\text{PM}_{2.5}$ was 89.5 and $85.9 \mu\text{g m}^{-3}$ in 2013 and 2014, respectively, 2.5 times the NAAQS ($35 \mu\text{g m}^{-3}$ as an annual average), indicating that Beijing is still facing severe fine particle pollution. While extensive studies have been conducted in recent years to characterize severe haze pollution (e.g., Guo et al., 2014; Huang et al., 2014; Sun et al., 2014; Zheng et al., 2015), most were carried out in a particular season. In reality, the very different compositions, sources, and evolution processes of severe haze pollution among the different seasons mean that a longer-term approach is needed to meet the challenge of mitigating fine particle pollution in Beijing.

A number of long-term measurements and source analyses have been conducted in Beijing during the last decade. Zhao et al. (2009) reported pronounced seasonal variations of $\text{PM}_{2.5}$, with higher concentrations in winter than summer. Similarly, Yang et al. (2011) conducted a long-term study of carbonaceous aerosol from 2005 to 2008 in urban Beijing. Both organic carbon (OC) and elemental carbon (EC) showed pronounced seasonal variations, with the highest concentrations occurring in winter and the lowest values in summer. A more detailed investigation of the chemical composition and sources of $\text{PM}_{2.5}$ in urban Beijing can be found in Zhang et al. (2013a). Sources of fine particles also vary greatly among the different seasons; for instance, coal combustion during periods requiring more domestic heating, biomass burning in harvest seasons, and dust storms in spring (Zheng et al., 2005; R. Zhang et al., 2013). Despite this, most previous long-term studies either focused on limited aerosol species, relied upon weekly filter samples, or used 1 month's worth of data to represent an entire season (R. Zhang et al., 2013; Y. Zhang et al., 2013). Therefore, our understanding of the full spectrum of seasonal variations of aerosol species and sources remains quite poor.

The Aerodyne aerosol mass spectrometer (AMS) is unique in its ability to provide real-time, online measurements of size-resolved submicron aerosol composition (Jayne et al., 2000; Canagaratna et al., 2007). While the AMS has been widely used in China in recent years (J. Xu et al., 2014, and references therein), real-time, long-term measurements of aerosol particle composition are still rare. Y. Zhang et al. (2013) conducted a 4-month measurement campaign of submicron aerosol composition and size distributions using a quadrupole AMS in urban Beijing. Their results showed higher concentration of organics during wintertime and secondary inorganic species in summer. Furthermore, positive matrix factorization (PMF) analysis of organic aerosol (OA) showed higher primary OA (POA) in winter and secondary OA (SOA) in summer. However, measurements over only 1

month or even less were conducted for each season, due to the high cost and maintenance of the AMS. The recently developed Aerosol Chemical Speciation Monitor (ACSM) is specially designed for long-term routine measurements of submicron aerosol composition (Ng et al., 2011). The ACSM has been proven reliable by several recent long-term field measurements, e.g., in Paris (Petit et al., 2015), north-central Oklahoma (Parworth et al., 2015), and Santiago de Chile (Carbone et al., 2013). Although the ACSM has been deployed at various sites in China (Sun et al., 2012, 2013b; Zhang et al., 2015), long-term measurements have yet to be reported.

In this study, the first of its kind, we conducted long-term, real-time measurements of non-refractory submicron aerosol (NR- PM_{1}) composition with an ACSM in Beijing, China, from July 2011 to June 2012. The seasonal variations of mass concentration and composition of submicron aerosol were characterized, and the diurnal cycles of aerosol species during the four seasons elucidated. The effects of meteorological parameters, particularly relative humidity and temperature, on aerosol composition and formation mechanisms were investigated. Finally, the potential source areas leading to high concentrations of aerosol species during the four seasons were investigated via potential source contribution function (PSCF) analysis.

2 Experimental methods

2.1 Sampling site

The ACSM was deployed on the roof of a two-story building (~ 8 m) at the Institute of Atmospheric Physics (IAP), Chinese Academy of Sciences ($39^{\circ}58'28''$ N, $116^{\circ}22'16''$ E, Fig. 1a) from July 2011 to June 2012. The sampling site is located between the north third and fourth ring road in Beijing, which is a typical urban site with influences from local traffic and cooking sources (Sun et al., 2012). The wind rose plots (Fig. 1b) show that southwesterly winds dominate all seasons except winter, when northwesterly and northerly winds prevail. The spring and fall seasons are also characterized by high frequencies of northwesterly and northerly winds. Also note that the prevailing winds with high wind speeds are more frequent during winter and spring than summer.

The meteorological parameters, including wind speed (WS), wind direction, relative humidity (RH), and temperature (T) were obtained from a 325 m meteorological tower at the same location. The parameters of pressure (P), solar radiation (SR), and precipitation were obtained from a ground meteorological station located nearby. The monthly variations of these meteorological parameters are presented in Fig. 2. Pronounced seasonal variations were observed for all meteorological parameters except WS. RH averaged at $> \sim 60\%$ in summer and presented its minimum value ($< 30\%$) in February. Temperature and solar radiation

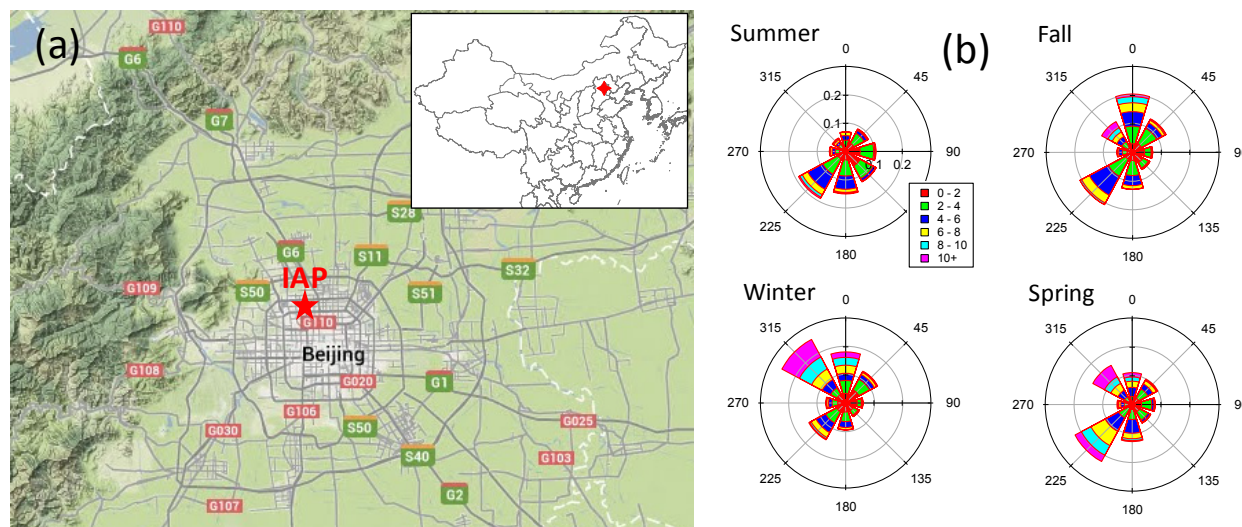


Figure 1. (a) Map of the sampling site (IAP). (b) Wind rose plots, color-coded by wind speed (m s^{-1}) for each season. The frequencies are set to the same scales for all seasons.

showed similar seasonal cycles, with high values in summer and low values in winter. The monthly variations of WS were relatively flat, yet slightly higher values in spring were observed. In addition, a considerable amount of precipitation was observed from June to August, yet it was negligible during wintertime.

2.2 Aerosol and gas measurements

The submicron aerosol particle composition including organics, sulfate, nitrate, ammonium, and chloride was measured in situ by the ACSM at a time resolution of ~ 15 min. The ACSM, built upon previous AMSs (Jayne et al., 2000; Drewnick et al., 2005; DeCarlo et al., 2006), is specially designed for long-term routine measurements of fine particle composition (Ng et al., 2011). The ACSM has been successfully deployed at various sites for chemical characterization of submicron aerosol (Ng et al., 2011; Budisulistiorini et al., 2013; Carbone et al., 2013; Sun et al., 2013b; Parworth et al., 2015). In this study, ambient aerosol particles were delivered to the sampling room through a stainless steel tube (outer diameter: 1.27 cm) with a flow rate of $\sim 3 \text{ L min}^{-1}$, out of which $\sim 84 \text{ cc min}^{-1}$ was sampled into the ACSM. A $\text{PM}_{2.5}$ URG cyclone (URG-2000-30ED) was installed in front of the sampling line to remove coarse particles ($> 2.5 \mu\text{m}$). To reduce the uncertainties of collection efficiency (CE), a silica gel diffusion dryer was set up in the front of the ACSM to ensure that the aerosol particles sampled were dry ($< 40\%$). The ACSM was calibrated routinely with pure ammonium nitrate particles for the response factor following the procedures detailed in Ng et al. (2011). A more detailed description of the ACSM calibration is given in Sun et al. (2012). It should be noted that we did not calibrate the ACSM with $(\text{NH}_4)_2\text{SO}_4$ to determine the relative ionization efficiency

(RIE) of sulfate since such an approach was only proposed recently. Using the method suggested by Budisulistiorini et al. (2014), the RIE of sulfate was estimated to be 1.1–1.6 during four seasons, leading to a highest uncertainty of 35 % in sulfate quantification. Considering that aerosol particle acidity may vary largely between different seasons, the method of Budisulistiorini et al. (2014) may introduce additional uncertainties in sulfate quantification. Therefore, we kept the default RIE of sulfate for the data analysis in this study.

2.3 ACSM data analysis

The ACSM data were analyzed for the mass concentrations of NR- PM_{10} species including organics, sulfate, nitrate, ammonium, and chloride using ACSM standard data analysis software. The RH in the sampling line, aerosol particle acidity and the fraction of ammonium nitrate (f_{AN}) in NR- PM_{10} are three major factors affecting the uncertainties of CE (Huffman et al., 2005; Matthew et al., 2008; Middlebrook et al., 2012). Because aerosol particles were dry and overall neutralized for most of the time, except some periods when the ratio of measured NH_4^+ to predicted NH_4^+ (i.e., $2 \times \text{SO}_4^{2-} / 96 \times 18 + \text{NO}_3^- / 62 \times 18 + \text{Cl}^- / 35.5 \times 18$) (Zhang et al., 2007) was less than 0.8, the composition-dependent CE recommended by Middlebrook et al. (2012), which is $\text{CE} = \max(0.45, 0.0833 + 0.9167 \times f_{\text{AN}})$, was used in this study. The validity of the ACSM data using variable CE in summer and winter was reported previously in Sun et al. (2012, 2013b) by comparing the NR- PM_{10} with $\text{PM}_{2.5}$ mass concentration measured by a TEOM system. The correlation between NR- PM_{10} and $\text{PM}_{2.5}$ for the entire year is shown in Fig. S1 in the Supplement. The variation of measured NR- PM_{10} tracked well with that of $\text{PM}_{2.5}$ overall, and yet showed different slopes in different seasons. The aver-

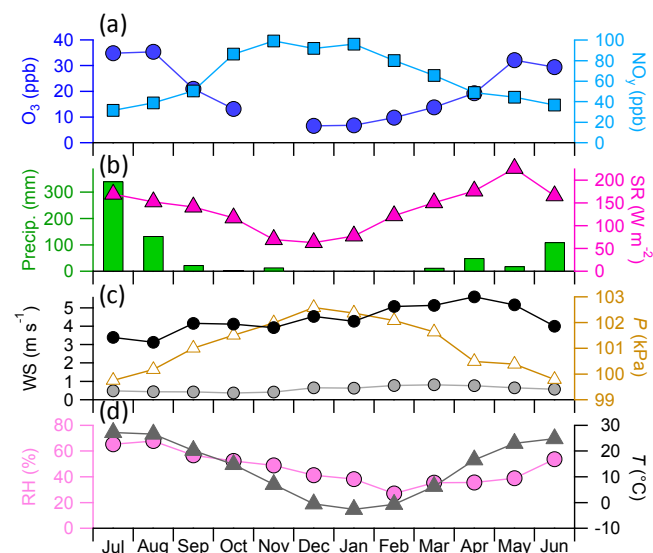


Figure 2. Monthly variation of (a) gaseous O₃ and NO_y, (b) precipitation (Precip.) and solar radiation (SR), (c) wind speed (WS) and pressure (*P*), and (d) relative humidity (RH) and temperature (*T*). The WS at the heights of 8 m (solid gray circles) and 240 m (solid black circles) are shown in (c).

age ratio of NR-PM₁ / PM_{2.5} for the entire year was 0.77 ($r^2 = 0.66$). It should be noted that the PM_{2.5} was measured by a heated TEOM (50 °C), which might have caused significant losses of semi-volatile species, e.g., ammonium nitrate and semi-volatile organics. For example, Docherty et al. (2011) found an average loss of ~44 % PM_{2.5} mass through use of the heated TEOM compared to that measured with a filter dynamics measurement system. Assuming that the average loss of PM_{2.5} mass by the heated TEOM is 30–50 %, the NR-PM₁ / PM_{2.5} ratio for the entire study would be ~0.5–0.6, which is close to that reported in Y. Zhang et al. (2013). Figure S1 also shows large variations of NR-PM₁ / PM_{2.5} ratios in the different seasons. The reasons for the variations include: (1) the ACSM cannot detect refractory black carbon, mineral dust, and metals. For example, low ratios of NR-PM₁ / PM_{2.5} (< 0.3) were observed during dust storm periods, when mineral dust is the dominant component of fine particles; (2) the contribution of semi-volatile species to PM_{2.5} varied greatly among the different seasons; and (3) the contribution of particles in the range of 1–2.5 μm to the total PM_{2.5} might also be different among different pollution episodes.

2.4 PSCF analysis

The 72 h back trajectories arriving at the IAP study site at a height of 300 m were calculated every 3 h for the entire study period using the National Oceanic and Atmospheric Administration Hybrid Single-Particle Lagrangian Integrated Trajectory model, version 4.8; Draxler and Rolph, 2003).

Each trajectory contained a series of latitude–longitude coordinates every 1 h backward in time for 72 h. If a trajectory end point falls into a grid cell (*i*, *j*), the trajectory is assumed to collect material emitted in the cell (Polissar et al., 1999). The number of end points falling into a single grid cell is n_{ij} . Some of these trajectory end points are associated with the data with the concentration of aerosol species higher than a threshold value. The number of these points is m_{ij} . The potential source contribution function (PSCF) is then calculated as the ratio of the number of points with concentration higher than a threshold value (m_{ij}) to the total number of points (n_{ij}) in the *ij*th grid cell. Higher PSCF values indicate higher potential source contributions to the receptor site. In this study, the domain for the PSCF was set in the range of (34–44° N, 110–124° E). The 75th percentile for each aerosol species during the four seasons (Table S1) was used as the threshold value to calculate m_{ij} . To reduce the uncertainties of m_{ij}/n_{ij} for those grid cells with a limited number of points, a weighting function (w_{ij}) recommended by Polissar et al. (1999) was applied to the PSCF in each season.

$$w_{ij} = \begin{cases} 1.00 & 80 < n_{ij} \\ 0.70 & 20 < n_{ij} \leq 80 \\ 0.42 & 10 < n_{ij} \leq 20 \\ 0.05 & n_{ij} \leq 10 \end{cases} \quad (1)$$

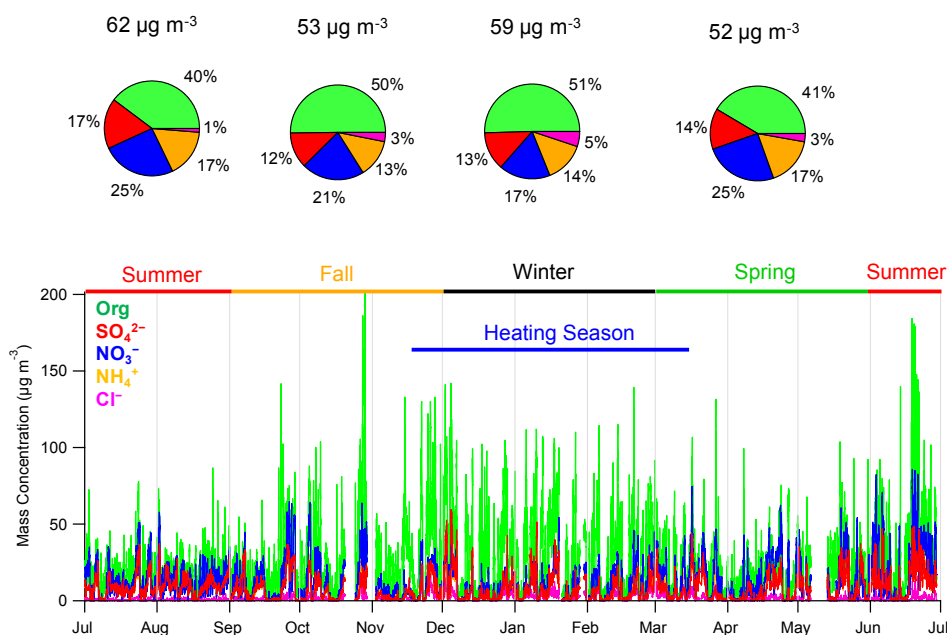
3 Results and discussion

3.1 Mass concentration and chemical composition

The average mass concentration of NR-PM₁ was 62 μg m⁻³ in summer (Fig. 3), which is higher than the 50 μg m⁻³ for July–August 2011 reported in Sun et al. (2012) due to the biomass burning impacts in June 2012 (Fig. S2). The summer NR-PM₁ level is close to that measured by a high-resolution aerosol mass spectrometer during the Beijing 2008 Olympic Games (Huang et al., 2010), but ~20 % lower than that determined in summer 2006 (Sun et al., 2010). The average NR-PM₁ mass concentrations were relatively similar during the other three seasons, varying from 52 to 59 μg m⁻³ and with slightly higher concentration during wintertime (Fig. 3). The NR-PM₁ measured in urban Beijing is overall higher than those previously reported in the Yangtze River Delta (YRD) region (27–43 μg m⁻³) (Huang et al., 2012, 2013; Zhang et al., 2015) and Pearl River Delta (PRD) region (31–48 μg m⁻³) (He et al., 2011; Huang et al., 2011; Gong et al., 2012), indicating more severe submicron aerosol pollution in Beijing compared to other places in China. Indeed, the annual average NR-PM₁ concentration (57 μg m⁻³) was much higher than the China NAAQS of PM_{2.5} (35 μg m⁻³ as an annual average). Assuming a similar PM_{2.5} level as that (89.5 μg m⁻³) in Beijing in 2013, NR-PM₁ on average accounted for 64 % of PM_{2.5}, which is overall consistent with

Table 1. Summary of mass concentrations of NR-PM₁ species, gaseous pollutants and meteorological parameters during the four seasons and entire study period.

	Entire study		Summer		Fall		Winter		Spring	
	mean	SD	mean	SD	mean	SD	mean	SD	mean	SD
Org ($\mu\text{g m}^{-3}$)	25.7	22.1	24.5	20.7	26.8	24.7	29.6	24.8	21.7	16.0
SO ₄ ²⁻ ($\mu\text{g m}^{-3}$)	8.1	8.3	10.6	8.2	6.5	7.5	7.7	9.2	7.3	7.6
NO ₃ ⁻ ($\mu\text{g m}^{-3}$)	12.6	12.8	15.6	14.4	11.4	12.7	10.3	9.5	13.1	13.4
NH ₄ ⁺ ($\mu\text{g m}^{-3}$)	8.5	7.9	10.2	8.2	6.9	7.3	8.1	7.4	8.8	8.1
Cl ⁻ ($\mu\text{g m}^{-3}$)	1.8	2.5	0.8	1.5	1.7	2.7	3.0	3.0	1.5	1.9
NR-PM ₁ ($\mu\text{g m}^{-3}$)	56.6	48.2	61.6	48.8	53.3	49.7	58.7	50.5	52.3	42.7
SO ₂ (ppb)	16.2	14.0	5.4	0.8			25.3	16.0	11.5	8.3
CO (ppm)	1.5	1.3	1.8	1.3			1.7	1.6	1.2	1.0
NO (ppb)	30.0	43.0	7.8	10.8	41.9	51.2	50.9	50.9	19.8	30.0
NO _y (ppb)	64.0	55.5	35.6	17.9	77.8	63.1	89.1	66.6	54.0	43.3
O ₃ (ppb)	21.2	23.8	33.3	29.1	20.3	24.4	7.9	8.5	20.8	19.3
RH (%)	47.0	23.4	62.7	18.9	52.7	20.0	35.6	20.3	36.5	22.5
T (°C)	13.3	11.6	26.3	3.6	14.1	7.0	-1.3	3.4	14.6	8.4
WS, 8 m (m s ⁻¹)	1.2	0.8	1.0	0.5	0.9	0.7	1.4	1.0	1.4	0.9
WS, 240 m (m s ⁻¹)	4.4	3.0	3.5	2.3	4.1	2.7	4.6	3.4	5.3	3.3

**Figure 3.** Time series of NR-PM₁ species for the entire year. The pie charts show the average chemical composition of NR-PM₁ during the four seasons (summer, fall, winter, and spring).

the results reported in previous studies (Sun et al., 2012, 2013b; Y. Zhang et al., 2013).

As indicated in Fig. 4, the summer season showed the highest frequency with NR-PM₁ loading in the range of 30–60 $\mu\text{g m}^{-3}$ (36 % of the time), while the winter season presented the highest frequency of low mass loadings (< 20 $\mu\text{g m}^{-3}$, 34 % of the time) due to the prevailing north-

westerly winds (Fig. 1b). However, high NR-PM₁ loading (> 90 $\mu\text{g m}^{-3}$) occurred 31 % of the time during the winter season, substantially more than during any of the other seasons (25, 25, and 21 % during summer, fall, and spring, respectively), indicating that heavy pollution occurred more frequently during winter than the other seasons. The fall and spring seasons showed similar variations of frequencies,

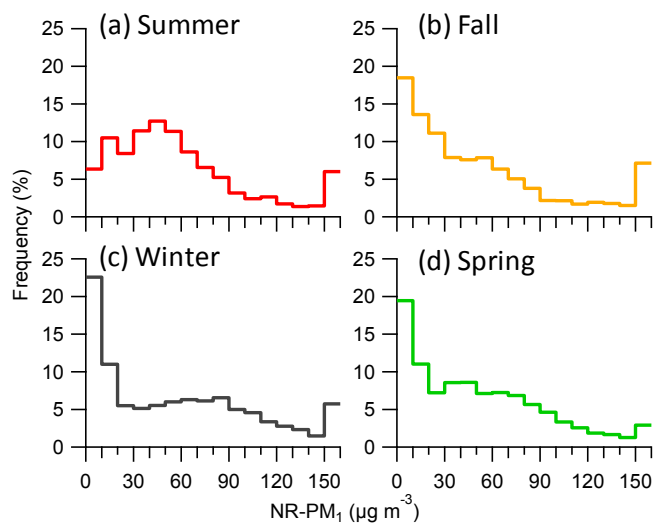


Figure 4. Frequency of NR-PM₁ mass loadings during the four seasons: (a) summer; (b) fall; (c) winter; (d) spring. Note that the frequency was calculated with 15 min average data.

which overall decreased monotonically as a function of NR-PM₁ loadings. Note that heavily polluted events, with NR-PM₁ mass concentrations larger than $150 \mu\text{g m}^{-3}$, occurred during all seasons, on average accounting for 3–7 % of the total time. Such heavily polluted events were mainly caused by agricultural burning in summer and fall, and coal combustion in winter, particularly under stagnant meteorological conditions (Sun et al., 2013b; Cheng et al., 2014).

The NR-PM₁ species varied dramatically and differently during the four seasons (Fig. 3). Overall, organics dominated NR-PM₁ during all seasons, accounting for 40–51 % on average. The dominance of organics in NR-PM₁ has been widely observed at various sites in China, e.g., 31–52 % in the YRD region (Huang et al., 2012, 2013; Zhang et al., 2015), 36–46 % in the PRD region (He et al., 2011; Huang et al., 2011; Gong et al., 2012), and 47 % in northwest China (J. Xu et al., 2014). Organics showed the largest contribution to NR-PM₁ in winter due to a large amount of carbonaceous aerosol emitted from coal combustion (Chen et al., 2005; Zhang et al., 2008). This is also consistent with the highest contribution of chloride, with coal combustion being a major source in winter (Zhang et al., 2012). High concentrations of organics were also observed during late June and early October, due to the impacts of agricultural burning in these 2 months. Secondary inorganic aerosol (SIA, i.e., sulfate + nitrate + ammonium) contributed the largest fraction of NR-PM₁ during the summer season (59 %) and the lowest fraction during the winter season (44 %). Such seasonal differences in PM composition reflect the different roles played by primary emissions and secondary formation. While photochemical production of secondary aerosol associated with higher O₃ and stronger solar radiation (Fig. 2) plays a dominant role in affecting aerosol composition in summer, primary emissions play an

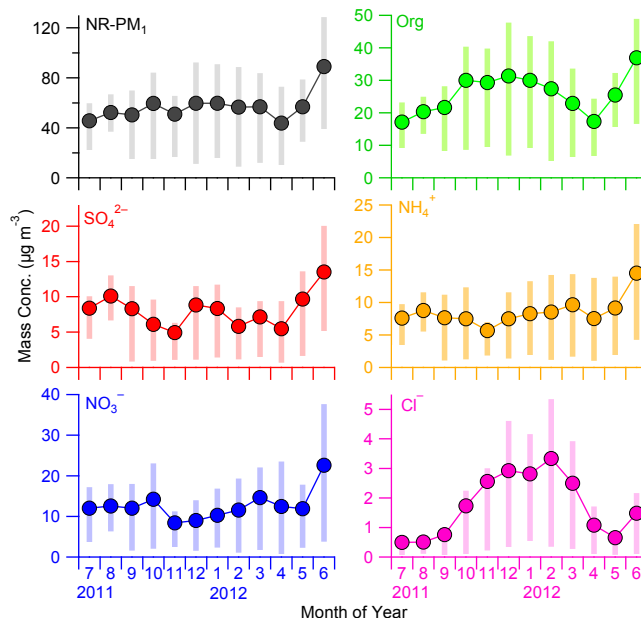


Figure 5. Seasonal variation of non-refractory submicron aerosol species. The bars represent the 25th and 75th percentiles, and the solid circles show mean values.

enhanced role in winter when photochemical processing is weaker (Sun et al., 2013b). It is interesting to note that nitrate, on average, showed a higher contribution than sulfate during the four seasons. Compared to previous AMS measurements in Beijing (Huang et al., 2010; Sun et al., 2010), the nitrate contribution to NR-PM₁ appears to show an increasing trend. The ratio of $\text{NO}_3^- / \text{SO}_4^{2-}$ varied from 1.3 to 1.8 in this study, which is overall higher than those (0.8–1.5) observed during the four seasons in 2008 (Y. Zhang et al., 2013). This result likely indicates a response of secondary inorganic aerosol composition to the variations of precursors of NO_x and SO₂ in recent years. For instance, a continuous effort to reduce SO₂ emissions is accompanied with a gradual increase in NO_x emissions (S. X. Wang et al., 2014), which results in an increasingly more important role played by nitrate in PM pollution in Beijing. Indeed, a recent model analysis of the response of SIA to their precursors from 2000 to 2015 showed that the increase of nitrate would exceed the reduction of sulfate in northern China, assuming no change to NH₃ emissions (Wang et al., 2013). A higher concentration of nitrate than sulfate has also been frequently observed at urban and rural sites in China in recent years, e.g., Nanjing, in the YRD region (Zhang et al., 2015), and Changdao Island (Hu et al., 2013).

3.2 Seasonal variation

The monthly average NR-PM₁ mass concentration stayed relatively constant throughout the year, with the average value ranging from 46 to $60 \mu\text{g m}^{-3}$, except in June 2012

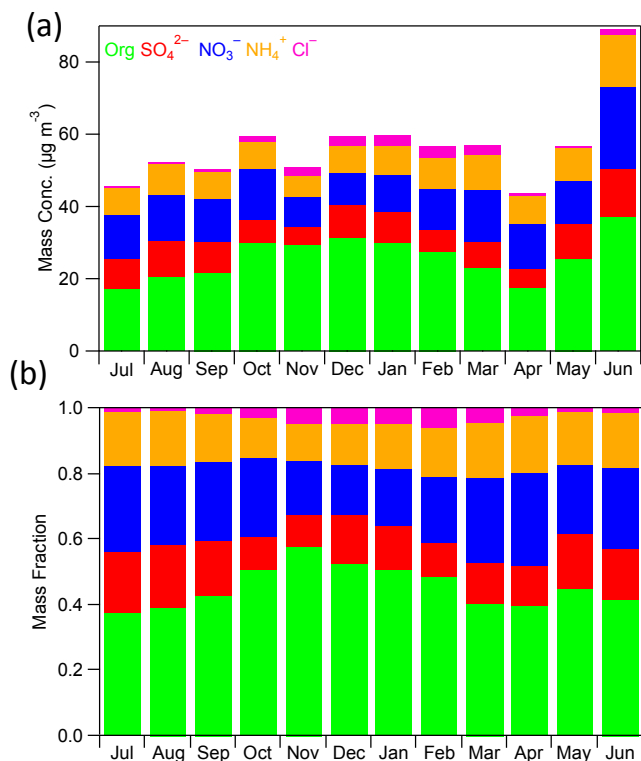


Figure 6. Monthly variation of (a) mass concentrations and (b) mass fractions of NR-PM₁ species.

(Fig. 5). The month of June presented the highest NR-PM₁ ($89 \mu\text{g m}^{-3}$) due to the impact of agricultural burning. Consistently, a higher concentration of NR-PM₁ was observed in the summer of 2008 (5 June–3 July) than the other seasons in Beijing (Y. Zhang et al., 2013). Zhao et al. (2009) also observed the highest concentration of PM_{2.5} in June 2007, due to the influences of agricultural burning. These results indicate that agricultural burning is a large source of PM pollution in Beijing in summer. The lowest concentration of NR-PM₁ in summer occurred in July, mainly due to abundant precipitation and high temperatures, which facilitated wet scavenging and convection of PM, respectively (Fig. 2). Similarly lower concentrations of PM_{2.5} in summer than in the other seasons were also observed previously at an urban site in Beijing (Zhao et al., 2009).

Among the NR aerosol species, organics and chloride presented pronounced seasonal variations, showing higher concentrations in winter than in the other seasons (Fig. 5). The concentration of organics increased from $17 \mu\text{g m}^{-3}$ in July to $\sim 30 \mu\text{g m}^{-3}$ in October, and then remained relatively stable across the whole of wintertime. The concentration of organics reached a minimum in April ($17 \mu\text{g m}^{-3}$), and then rapidly increased to $37 \mu\text{g m}^{-3}$ in June. Correspondingly, the contribution of organics to NR-PM₁ increased from $\sim 40\%$ in summer to above 50% during wintertime (Fig. 6). A higher concentration of carbonaceous aerosol in winter, com-

pared to the other three seasons, was also observed in Beijing (R. Zhang et al., 2013; Zhao et al., 2013). The seasonal variation of organics is primarily driven by emissions from various sources and secondary production. While the POA, particularly from coal combustion emissions, is significantly elevated during wintertime, the photochemically processed SOA dominates OA in summer (Sun et al., 2012, 2013b). In the present study, chloride showed a similar seasonal variation to that of organics. The chloride concentration during wintertime ($2.8\text{--}3.3 \mu\text{g m}^{-3}$) was approximately 6 times that ($0.5 \mu\text{g m}^{-3}$) in summer. The contribution of chloride to NR-PM₁ showed a similar seasonal trend, with the lowest contribution in summer ($\sim 1\%$) and the highest in winter ($\sim 5\text{--}6\%$) (Fig. 6). High concentrations of chloride in winter are associated with enhanced coal combustion emissions (Sun et al., 2013b), but also with low ambient temperature, which facilitates the formation of particle-phase ammonium chloride. Also note that chloride showed a twice as high concentration and contribution in June than the other 2 months in summer because agricultural burning is also a large source of chloride (Viana et al., 2008; Cheng et al., 2014).

The seasonal variation of sulfate is different from organics and chloride. The sulfate concentration gradually decreased from $10.1 \mu\text{g m}^{-3}$ in August to $4.9 \mu\text{g m}^{-3}$ in November, which was associated with a synchronous decrease in solar radiation and O₃ (Fig. 2). The contribution of sulfate to NR-PM₁ showed a corresponding decrease from 19 to 10%. The sulfate concentration then increased to $8.3\text{--}8.8 \mu\text{g m}^{-3}$ in December and January, likely due to a significant increase of precursor SO₂ associated with an increased demand for domestic heating during the winter season, which can be oxidized to form sulfate via either gas-phase oxidation or aqueous-phase processing (W. Y. Xu et al., 2014). Sulfate showed the highest concentration in June ($13.5 \mu\text{g m}^{-3}$) due to secondary production, but possibly the impact of biomass burning as well. Indeed, a recent study in the YRD region also found a large enhancement of sulfate in biomass burning plumes in summer (Zhang et al., 2015). Nitrate showed minor seasonal variation, with the monthly average concentration ranging from 8 to $15 \mu\text{g m}^{-3}$, except in June ($23 \mu\text{g m}^{-3}$). It is interesting that a higher concentration of nitrate was observed in summer and spring than in winter. On average, nitrate accounted for $\sim 25\%$ of NR-PM₁ during summertime, but decreased to $\sim 15\%$ during wintertime (Fig. 6). Although high temperatures in summer favor the dissociation of ammonium nitrate particles to gas-phase ammonia and nitric acid, the correspondingly high RH and excess gaseous ammonia facilitate the transformation of nitric acid to aqueous NH₄NO₃ particles (Meng et al., 2011; Sun et al., 2012). The lowest concentration of nitrate during wintertime might be primarily caused by the weak photochemical production associated with low solar radiation and oxidants (e.g., O₃). In addition, the higher particle acidity in winter (Liu, 2012) and lower mixing ratio of gaseous ammonia may also suppress the formation of ammonium nitrate particles

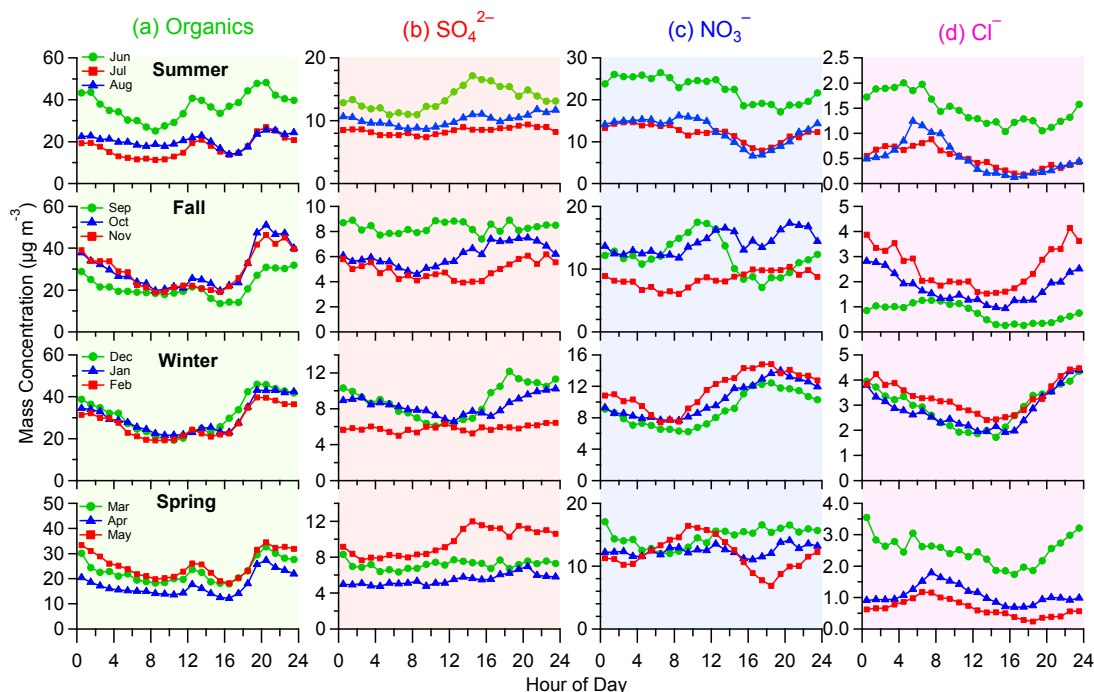


Figure 7. Monthly average diurnal cycle of (a) organics, (b) sulfate, (c) nitrate, and (d) chloride during the four seasons.

(Zhang et al., 2007). The seasonal variation of ammonium is similar to that of sulfate and nitrate because ammonium primarily exists in the form of NH_4NO_3 and $(\text{NH}_4)_2\text{SO}_4$.

3.3 Diurnal variations

As demonstrated in Fig. 7, the diurnal cycles of organics during the four seasons were overall similar, characterized by two pronounced peaks occurring at noon and during the evening. PMF analysis of OA suggested that the noon peak was primarily caused by cooking emissions, while the evening peak was driven by different primary emissions (e.g., cooking, traffic, and coal combustion emissions) among the different seasons (Sun et al., 2012, 2013b). It should be noted that the noon peak in summer was more significant than in fall and winter. Indeed, the cooking emissions, determined by subtracting the background (10:00–11:00) from the noon peak (12:00–13:00), were $\sim 1.5\text{--}2\ \mu\text{g m}^{-3}$ from September to the following March, which were lower than the $\sim 3.5\ \mu\text{g m}^{-3}$ calculated for June and July. This seasonal trend agreed with that of temperature, indicating that cooking emissions are temperature-dependent, probably because of increased cooking activity in hot summers than cold winters.

Relatively flat diurnal cycles were observed for sulfate during most months, indicating the regional characteristics of sulfate. In fact, multi-day build-up of sulfate was frequently observed during all seasons (Fig. 3), supporting the notion of regional influences on sulfate in Beijing. It should be noted

that the daytime photochemical production of sulfate from gas-phase oxidation of SO_2 might be masked by an elevated planetary boundary layer (PBL). Considering the dilution effect of the PBL, Sun et al. (2012) found that sulfate increased gradually from morning to late afternoon, demonstrating the daytime photochemical production of sulfate. In this study, sulfate in May, June and October showed an evident daytime increase until late afternoon, indicating an important role played by gas-phase photochemical processing in driving the sulfate diurnal cycle.

Nitrate showed substantially different diurnal cycles among different months. A clear daytime increase starting from about 08:00 to 19:00 was found in the 5 months of January, February, March, November and December, indicating that such a diurnal pattern is more significant during wintertime compared to the fall and spring seasons. Figure 2 shows that the temperature during these 5 months was generally low ($< 10\ ^\circ\text{C}$), under which the partitioning of NH_4NO_3 into gaseous NH_3 and HNO_3 would not be significant. As a result, photochemical production would be the primary factor driving the diurnal variations. The photochemical production rate calculated from the daytime increase was $0.6\text{--}0.8\ \mu\text{g m}^{-3}\ \text{h}^{-1}$ during winter and $\sim 0.2\text{--}0.3\ \mu\text{g m}^{-3}\ \text{h}^{-1}$ in November and March. Nitrate presented pronounced diurnal cycles in summer (June, July, and August), with the concentrations gradually decreasing during daytime and reaching a minimum at $\sim 16:00$. Similar diurnal cycles have been observed on many occasions in summer in Beijing (Huang et al., 2010; Sun et al., 2012; Zhang et al., 2015). The evap-

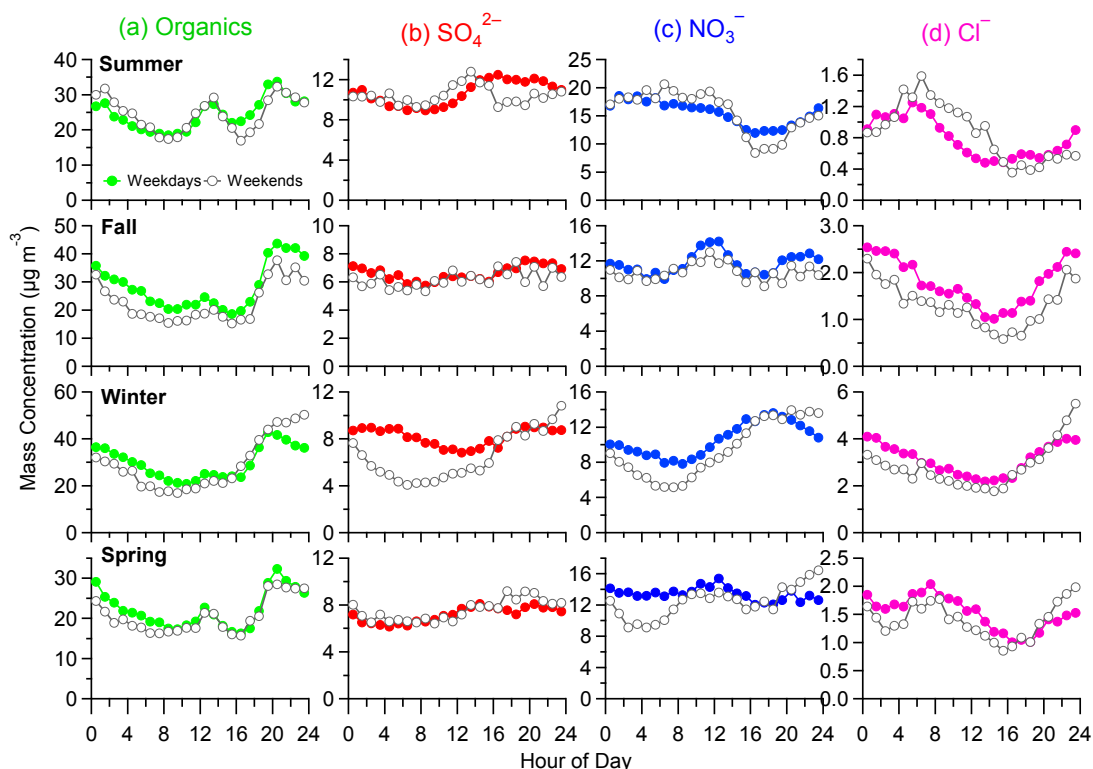


Figure 8. Comparison of the average diurnal cycles of (a) organics, (b) SO_4^{2-} , (c) NO_3^- , and (d) Cl^- between weekdays and weekends during the four seasons. Note that the periods with $\text{NR-PM}_{10} < 20 \mu\text{g m}^{-3}$ are excluded.

orative loss of NH_4NO_3 associated with high temperatures, which overcomes the amount of photochemical production, plays the major role in driving such diurnal cycles. The rising PBL plays an additional role in the low concentrations of nitrate during daytime (Sun et al., 2012). The diurnal cycle of nitrate in May and September was also significant, characterized by a pronounced morning peak occurring at $\sim 10:00$, when photochemical production dominated over the gas-particle partitioning of NH_4NO_3 . Nitrate showed a relatively flat diurnal cycle in April, indicating a combined effect of various nitrate formation mechanisms.

Chloride in this study was primarily detected as ammonium chloride because ACSM is insensitive to refractory NaCl and/or KCl at its vaporizer temperature of 600°C . As shown in Fig. 7, two different diurnal cycles were observed throughout different months. For the months of July, August, September, April, and May, chloride presented a morning peak when both temperatures and the PBL were at their lowest, and then rapidly decreased to a low ambient level at $\sim 18:00$. Such a diurnal cycle was likely primarily driven by temperature-dependent gas-particle partitioning (Hu et al., 2008). The diurnal cycles of chloride during the remaining months were also significant, all of which were characterized by high concentrations at night. Coincidentally, these months fell during the season of high domestic-heating de-

mand, which usually starts on 15 November and ends on 15 March. Coal combustion has been found to be a large source of chloride (Zhang et al., 2012; Sun et al., 2013b). Therefore, the diurnal cycle of chloride is likely dominantly driven by coal combustion emissions that are intensified at night for domestic heating.

3.4 Weekend effects

Because the switch between clean periods and pollution episodes arising from different source areas happens frequently in Beijing (Sun et al., 2013b; Guo et al., 2014), the diurnal cycles of aerosol species can vary greatly due to the influences of different occurrences of clean periods between weekdays and weekends (Sun et al., 2013b). Therefore, periods with low aerosol loadings ($\text{NR-PM}_{10} < 20 \mu\text{g m}^{-3}$) were excluded from the results (Fig. 8) for a better investigation of the weekend effects (for the average diurnal cycles with clean periods included, see Fig. S3). As shown in Fig. 8, there were no clear weekend effects in the summer, except for slightly lower concentrations of organics, sulfate, and nitrate in the late afternoon on weekends. This suggests that there are no significant differences in anthropogenic activity between weekdays and weekends in summer. Although some enhanced traffic emissions between 00:00 and 06:00 on weekends might have occurred, as indicated by the higher

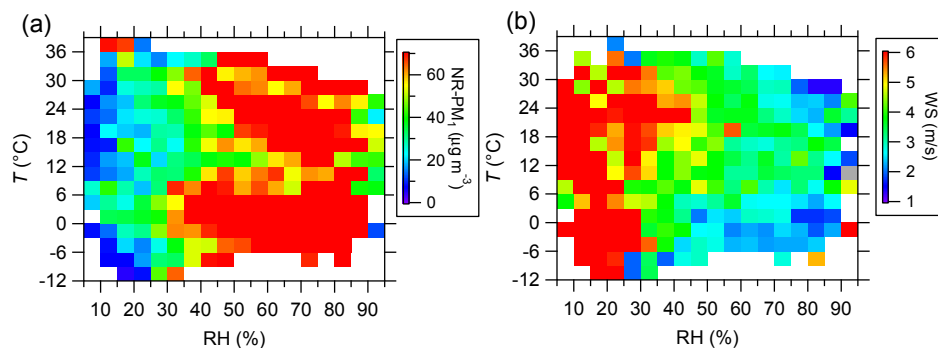


Figure 9. RH/ T dependence of (a) NR-PM₁ mass concentration and (b) WS for a whole year. The data are grouped into grids with increments of RH and T being 5 % and 3 °C, respectively. Grid cells with a number of data points fewer than 10 are excluded.

concentration of NO (Fig. S4), they appeared to have negligible impacts on secondary sulfate and nitrate. While the diurnal variations of organics and chloride were similar between weekdays and weekends during the fall season, sulfate and nitrate showed pronounced weekend effects, with persistently higher concentrations at weekends throughout the day. An explanation for this is the stronger photochemical production of secondary species associated with higher O₃ and solar radiation on weekends (Fig. S4). Consistently, SOA showed similar weekend effects as those of secondary inorganic species, while POA did not (Sun et al., 2015). Because of the regional characteristics of secondary aerosols, further analysis is needed to address the impacts of regional transport on the weekend effects of secondary species. Winter showed the most pronounced weekend effects for all aerosol species. All aerosol species showed much lower concentrations on weekends than on weekdays across the entire day, which was consistent with those of NO, SO₂, and CO (Fig. S4). These results clearly indicate much reduced anthropogenic activity on weekends during wintertime because of low ambient temperature (−4 to −3 °C). Further evidence is provided by the diurnal cycles of organics, which presented pronounced noon peaks on weekends during all seasons except winter. This observation was consistent with much reduced cooking activity on weekends during wintertime. Similar to summer, no evident weekend effects were observed in spring. The weekend effects of aerosol species in this study are overall consistent with those observed by Han et al. (2009), in which similar diurnal cycles of primary elemental carbon, CO, and CO₂ between weekdays and weekends under weak wind conditions were observed during the three seasons other than winter.

3.5 Meteorological effects

Figure 9 shows the RH- and T -dependent distributions of NR-PM₁ and WS for the entire year. The distribution of NR-PM₁ showed an obvious concentration gradient as a function of RH. NR-PM₁ showed the lowest mass loading, gen-

erally less than 20 μg m^{−3} at RH < 20 %, and had no clear dependence on T . This can be explained by the high WS (often larger than 5 m s^{−1}; Fig. 9b) at low RH levels associated with clean air masses from the north and/or northwest. Previous studies have also found a strong association between low aerosol loading and high WS in Beijing (Han et al., 2009; Sun et al., 2013b). NR-PM₁ showed moderately high concentrations (~20–40 μg m^{−3}) at low RH (20–40 %), which rapidly increased to a high concentration level (> 60 μg m^{−3}) at RH > 50 %. These results indicate that severe haze episodes in Beijing mostly occur under high humidity conditions, when WS is low as well. Two different regions with high concentrations of NR-PM₁ are apparent in Fig. 9a: one in the top-right region with high temperature (> ~15 °C), and another in the bottom-right region with low ambient temperature (< ~6 °C). Such a difference in distribution illustrates the severity of PM pollution in different seasons. Note that low concentrations of NR-PM₁ sometimes occurred at RH > 90 %, likely due to the scavenging of particles by rain or winter snow.

The RH- and T -dependent distributions of major aerosol species (Fig. 10) allow us to further investigate the RH/ T impacts on the formation of aerosol species. While all aerosol species showed similar concentration gradients as a function of RH to that of NR-PM₁, the T -dependent patterns varied greatly. Organics generally showed the highest concentrations under low T (< 6 °C) and high humidity conditions – very similar to the behavior of chloride, which is mainly derived from combustion sources, e.g., coal combustion or biomass burning (Zhang et al., 2012; Cheng et al., 2014). The results suggest that high concentrations of organics during wintertime are primarily caused by coal combustion emissions during the domestic-heating season, particularly from residential coal combustion (Zhang et al., 2008). In fact, a previous study by our group found that nearly one-third of OA during wintertime is primary coal combustion OA (CCOA) (Sun et al., 2013b). In contrast, organics showed much lower concentrations under the conditions of higher RH and higher T , for which one of the reasons was prob-

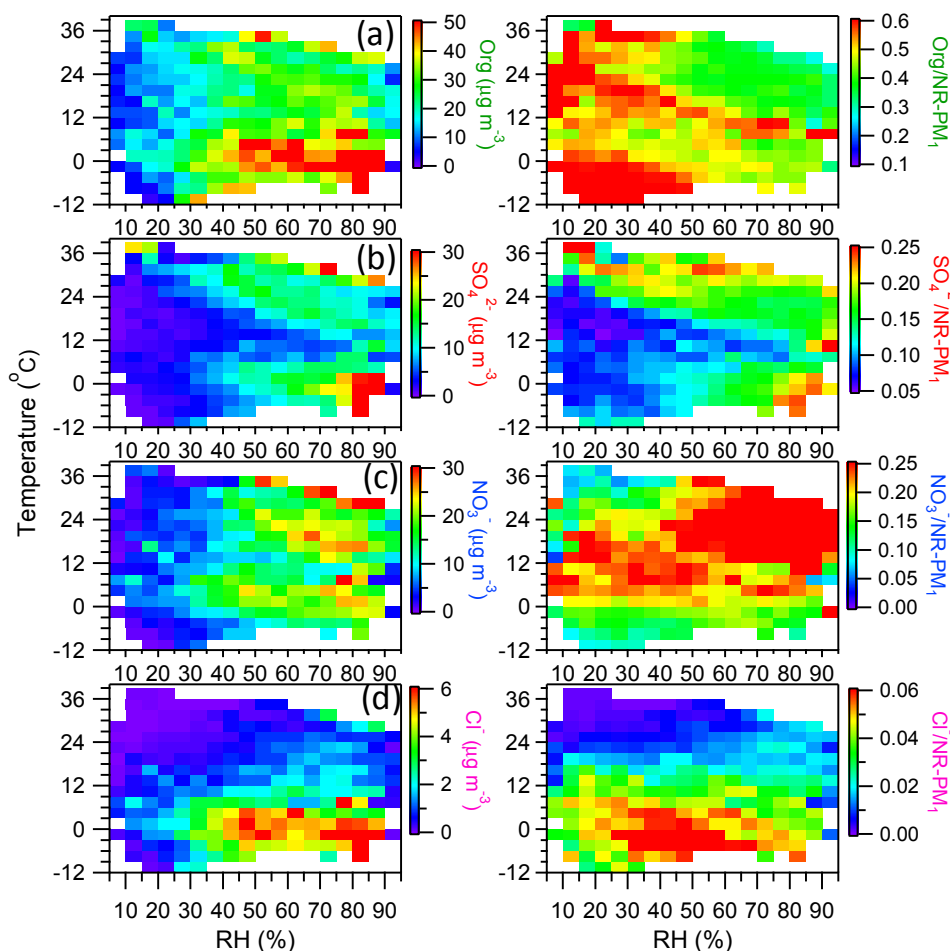


Figure 10. RH/ T dependence of mass concentrations and mass fractions of aerosol species for a whole year: (a) organics; (b) sulfate; (c) nitrate; (d) chloride. The data are grouped into grids with increments of RH and T being 5 % and 3 °C, respectively. Grid cells with a number of data points fewer than 10 are excluded.

ably far fewer coal combustion emissions during summertime (Zheng et al., 2005; R. Zhang et al., 2013). Consistently, CCOA has not yet been resolved from PMF analyses of AMS OA in summer in Beijing (Huang et al., 2010; Sun et al., 2010). Note that the region with a high concentration of organics corresponded to a high concentration of NR-PM₁. In this region, organics accounted for the largest fraction of NR-PM₁ (approximately 40–50 %), indicating that severe PM pollution under low temperature and high humidity conditions is dominantly contributed to by organics. The mass fraction of organics, however, showed an opposite distribution to that of mass loading. As shown in Fig. 10, organics presents the highest contribution to NR-PM₁ ($\sim > 50\%$) in the left-hand region with low RH, indicating the dominance of organics during periods with low NR-PM₁ mass loadings. Such a distribution is independent of temperature, suggesting a ubiquitously organics-dominant composition during clean days in all seasons.

The RH/ T dependence of secondary inorganic species showed somewhat different behaviors from that of organics. Sulfate presented two high concentration regions, with the highest values occurring during wintertime when T was below 0 °C and RH was above 70 %. Aqueous-phase oxidation, mostly fog processing, has been found to play a dominant role in sulfate formation under such meteorological conditions (Sun et al., 2013a). Surprisingly, the semi-volatile nitrate showed a relatively homogeneous distribution across different temperatures at RH > 40 %. Despite high temperature in summer, high humidity facilitates the transformation of gaseous species into aqueous-phase nitrate particles (Sun et al., 2012), particularly in the presence of high abundance of gaseous ammonia (Ianniello et al., 2010). In fact, nitrate showed the highest contribution ($> \sim 25\%$) to NR-PM₁ mass under high T and high RH conditions, which were also the conditions under which high concentrations of NR-PM₁ were observed. The fact that nitrate contributed more than sulfate ($\sim 15\text{--}20\%$) to NR-PM₁ mass during these condi-

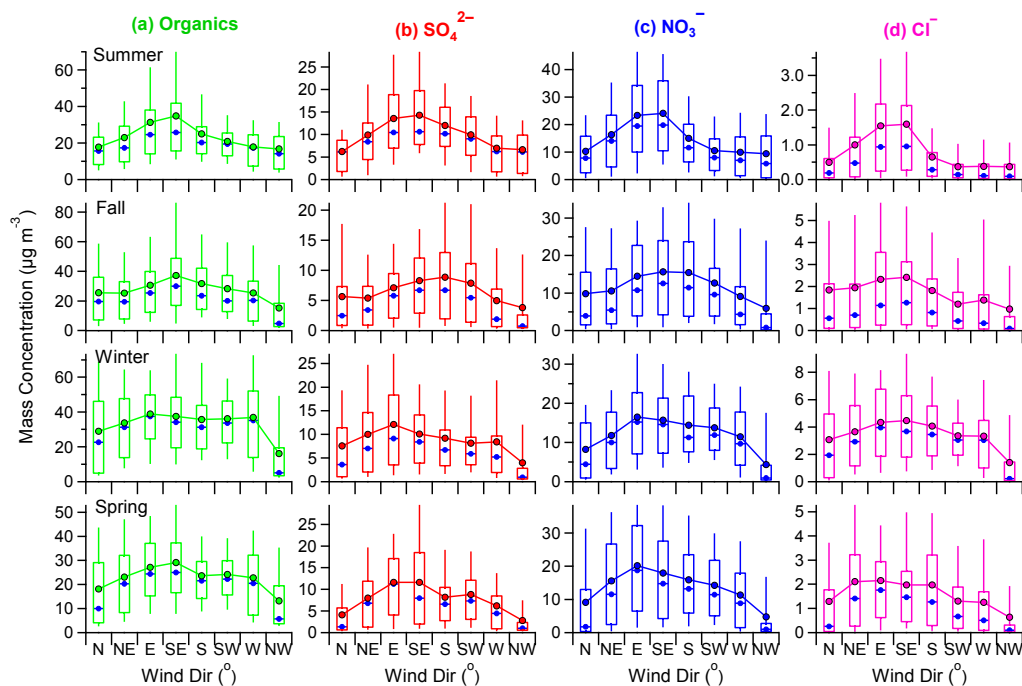


Figure 11. Box plots of mass concentrations of (a) organics, (b) SO_4^{2-} , (c) NO_3^- , and (d) Cl^- as a function of wind direction (Dir) sectors. All the data were segregated into eight wind sectors representing north (N), northeast (NE), east (E), southeast (SE), south (S), southwest (SW), west (W), and northwest (NW). The mean (cross), median (horizontal line), 25th and 75th percentiles (lower and upper box), and 10th and 90th percentiles (lower and upper whiskers) are shown.

tions suggests an important role played by nitrate in summer haze formation. While the concentration of nitrate at various temperatures was similar, its contribution to NR-PM₁ was generally lower at low temperatures due to the greater enhancement of organics during wintertime. Also note that the two semi-volatile species, i.e., nitrate and chloride, show the lowest contributions to NR-PM₁ in the top-left region with the highest T and lowest RH. This illustrates the evaporative loss process of ammonium nitrate and ammonium chloride under high temperatures in summertime. However, sulfate shows a relatively higher contribution in this region since ammonium sulfate is less volatile than ammonium nitrate and chloride (Huffman et al., 2009).

3.6 Source analysis

In summer, all NR-PM₁ species showed evident wind sector gradients, with higher concentrations in association with winds from the east (E) and southeast (SE), and lower concentrations with northwest (NW) wind (Fig. 11). The average NR-PM₁ concentration from the SE was $89.5 \mu\text{g m}^{-3}$, which was more than twice that ($39.4 \mu\text{g m}^{-3}$) from the NW. All aerosol species increased as wind sectors changed along the N–NE–E–SE gradient, and then decreased along the SE–S–SW–W gradient. Such wind sector dependence of aerosol composition is remarkably consistent with the spatial distribution of fine particles in Beijing in 2013 (Beijing Environ-

mental Statement 2013). These results suggest an inhomogeneous distribution of air pollution around the IAP sampling site in summer. Organics dominated NR-PM₁ across different sectors (37–43%), followed by nitrate (21–28%), sulfate (15–20%), and ammonium (15–17%). While chloride contributed a small fraction of NR-PM₁ (0.7–1.8%), the mass concentration showed the largest difference between SE and NW. The fall season showed a similar aerosol composition dependence as that in summer, with higher concentrations from the E, SE, and S. However, the gradients of wind sectors appeared to be smaller. For example, the average NR-PM₁ concentration ranged from 46.3 to $72.7 \mu\text{g m}^{-3}$ in all eight sectors except NW. Organics showed a similar dominance in NR-PM₁, accounting for 47–55%, and the contribution was ubiquitously higher than in summer for all wind sectors. It should be noted that the NW sector showed the largest difference between mean and median values for all species. The much lower median values suggest a dominance of clean days for most of the time in this sector. In contrast, the summer season showed higher median concentrations from the NW, indicating a higher regional background during this season. The winter season showed consistently high concentrations of PM across the different wind sectors, except for NW, where the mass concentrations were approximately half of those in the other sectors. The average NR-PM₁ ranged from 55.0 to $84.4 \mu\text{g m}^{-3}$, with organics being the major fraction, accounting for 46–54%. The spring

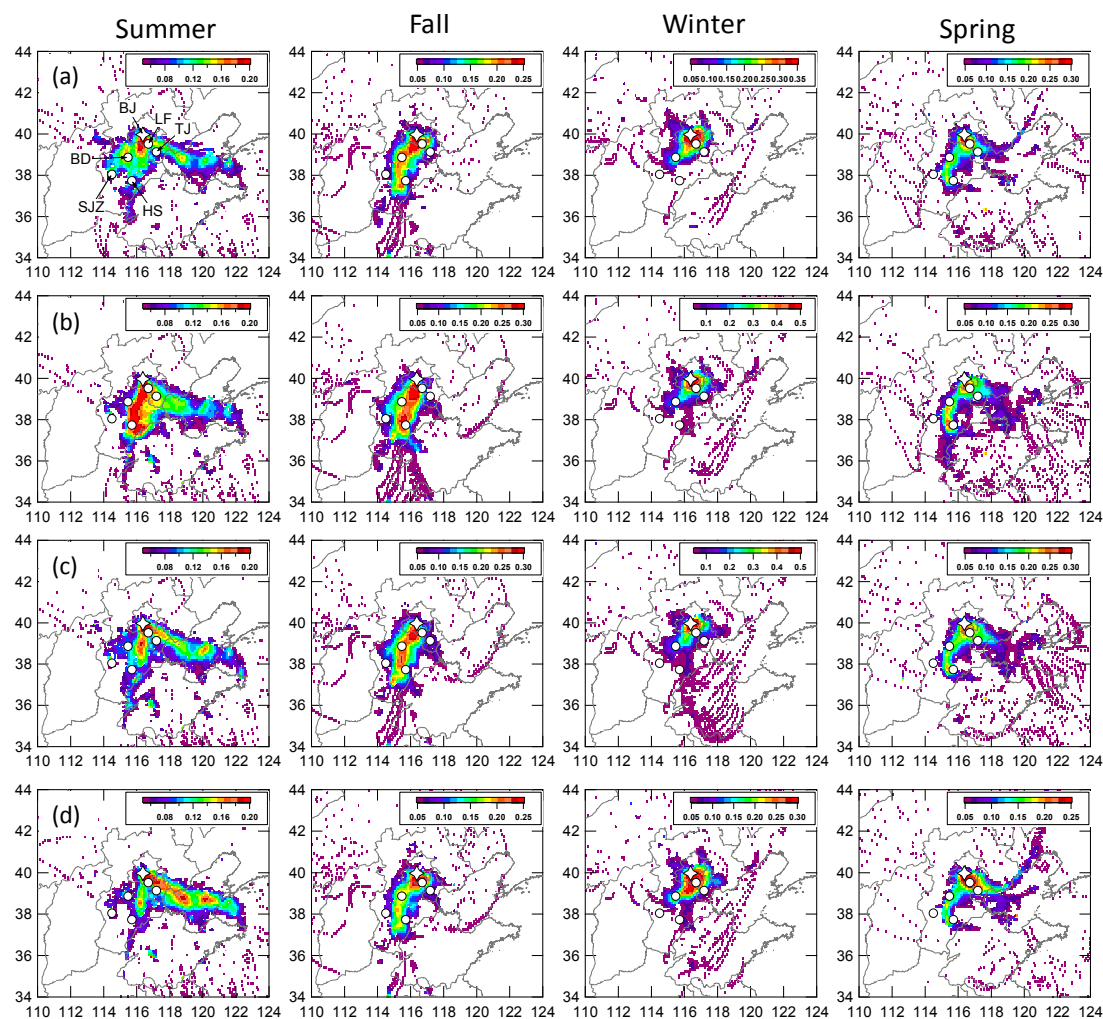


Figure 12. PSCF of NR-PM₁ species during four seasons: (a) organics; (b) sulfate; (c) nitrate; (d) chloride. The cities marked in each panel are Beijing (BJ), Tianjin (TJ), Langfang (LF), Baoding (BD), Shijiazhuang (SJZ), and Hengshui (HS). The color scales indicate the values of PSCF.

season showed a similar wind sector dependence on aerosol composition as the fall season. The average NR-PM₁ ranged from 49.0 to 74.4 $\mu\text{g m}^{-3}$ for all of the wind sectors, except the N (38.5 $\mu\text{g m}^{-3}$) and NW (24.7 $\mu\text{g m}^{-3}$) sectors which had much lower mass concentrations. Similar to other seasons, organics dominated NR-PM₁ throughout the different sectors (36–53 %), followed by nitrate (19–27 %), and sulfate (11–16 %).

As Fig. 12 shows, the potential source areas for aerosol species varied among the four seasons. In summer, high potential source areas were mainly located to the south, southwest, and southeast of Beijing. Organics had a relatively small potential source region in the south of Beijing (< 100 km) and a small source region located around Baoding – one of the most polluted cities in Hebei Province. A narrow and visible source area to the southeast of Beijing, including Tianjin and the Bohai Sea, was also observed. Nitrate and chloride showed similar source areas to organics.

The high potential source area to the southeast of Beijing was mainly caused by open agricultural burning in June in northern China. Sulfate showed a distinct source region characterized by a narrow high PSCF band along Hengshui–Baoding–Langfang–Beijing. Such a pollution band agrees well with the topography of the North China Plain, with the Taihang Mountains to the west and Yan Mountains to the north. The wide area of high PSCF for sulfate also indicates a regional characteristic of sulfate that is formed from gas-phase oxidation or cloud processing of precursor SO₂, which is particularly high in Hebei Province (Ji et al., 2014). Secondary nitrate showed a similar, yet much smaller, PSCF region compared to sulfate. One reason for this might be the evaporative loss of ammonium nitrate during the long-range transport in summer.

All aerosol species showed similar PSCF spatial distributions during the fall season, with high potential source regions located in a narrow area from Hengshui, Baoding to

Beijing. These results suggest that regional transport from the southwest plays a dominant role in formation of severe haze pollution in fall. The wintertime results showed largely different PSCF distributions from the other seasons. High PSCF values were mainly located in a small region (< 50 km) in the south and southeast of Beijing. Although Hebei Province often has worse air pollution than Beijing during wintertime (Ji et al., 2014), the cities far away from Beijing appear not to be a very important source of wintertime air pollution in Beijing. One explanation for this is that stagnant meteorological conditions occur more frequently in winter due to low WS and T inversions. Thus, local emissions and transport from nearby regions would play a more significant role in affecting the pollution level in Beijing. While the spring season showed similarly small potential source regions to those during wintertime, an obvious high potential source area in Hebei Province was also observed. The transport of air pollution from the SW to the NE along the Taihang Mountains in northern China has been observed many times in previous studies (L. T. Wang et al., 2014; Z. Wang et al., 2014). Given that many cities located on this pathway are often highly polluted, such as Shijiazhuang, Baoding, and Hengshui, regional transport from these areas would have a potentially high impact on the formation of severe haze pollution in Beijing.

4 Conclusions

This paper presents the results from a year-long, real-time measurement study of submicron aerosol particle composition using an ACSM, conducted at an urban site in Beijing from July 2011 to June 2012. The mass concentration of NR-PM₁ varied dramatically, with the seasonal average concentration ranging from 52 to 62 $\mu\text{g m}^{-3}$. Organics comprised a major fraction of NR-PM₁ during all seasons, accounting for 40–51 % on average. The average contribution of nitrate to NR-PM₁ (17–25 %) exceeded that of sulfate (12–17 %) during all seasons, suggesting an enhanced role of nitrate in PM pollution in recent years. Organics and chloride were two species showing pronounced seasonal variations in both mass concentrations and mass fractions. The higher concentrations of organics and chloride in winter than summer were largely due to enhanced coal combustion emissions. We also observed high concentrations of organics and chloride in June and October – 2 months with strong agricultural burning impacts. The seasonal variations of secondary sulfate and nitrate were not significant because of the large variations of precursor concentrations, photochemical production, and also meteorological effects in different seasons. However, higher contributions of SIA in summer (57–61 %) than in winter (43–46 %) were still observed, indicating a more significant role of secondary production in summer. The diurnal cycles of organics were similar during all seasons, all characterized by two pronounced peaks. While the diurnal cycles

of secondary sulfate were overall relatively flat during most months of the year, those of nitrate varied greatly in different seasons. It was evident that the diurnal cycles of nitrate are driven by gas-particle partitioning and daytime photochemical production in summer and winter, respectively. The winter season showed substantially different concentrations of aerosol species between weekdays and weekends, with much lower concentrations on weekends. However, no significant weekend effects were observed during the other seasons.

Meteorological conditions play an important role in the formation of severe PM pollution in Beijing. In this study, we have illustrated the influences of RH and T on aerosol loading and chemistry in different seasons. All aerosol species increased significantly under stagnant meteorological conditions associated with high RH and low WS. NR-PM₁ showed two high concentration regions ($> 60 \mu\text{g m}^{-3}$) at RH > 60 %. While organics comprised a major fraction of NR-PM₁ in these two regions, the abundances of sulfate and nitrate and air temperature were largely different, suggesting they play different roles in causing PM pollution during different seasons. Under drier conditions (RH < 30 %), the NR-PM₁ concentration was generally low and organics contributed more than 50 % of its mass, indicating the importance of organics during clean periods. The semi-volatile nitrate presented the largest contribution under high RH and high T , highlighting the importance of nitrate formation via aqueous-phase processing in summer. All NR-PM₁ species showed obvious dependence on wind direction, with higher concentrations commonly associated with winds from the S, E, and SE. This was consistent with the results from PSCF analysis, which showed that the high potential source areas were mainly located to the S and SW of Beijing. The high potential source areas varied differently during the four seasons. A common high potential source area to the SW of Beijing, along the Taihang Mountains, was observed during all seasons except winter, demonstrating the potentially high impact of regional transport on severe PM pollution in Beijing. The winter season showed a much smaller source region compared to the other seasons, indicating that local and regional transport over a smaller regional scale are more important. High potential source areas to the SE of Beijing were also observed for organics, nitrate, and chloride in summer, likely due to agricultural burning.

The Supplement related to this article is available online at doi:10.5194/acp-15-10149-2015-supplement.

Acknowledgements. This work was supported by the National Key Project of Basic Research (2014CB447900; 2013CB955801), the Strategic Priority Research Program (B) of the Chinese Academy of Sciences (XDB05020501), and the National Natural Science Foundation of China (41175108).

Edited by: W. Maenhaut

References

- Budisulistiorini, S. H., Canagaratna, M. R., Croteau, P. L., Marth, W. J., Baumann, K., Edgerton, E. S., Shaw, S., Knipping, E. M., Worsnop, D. R., and Jayne, J. T.: Real-time continuous characterization of secondary organic aerosol derived from isoprene epoxydiols (IEPOX) in downtown Atlanta, Georgia, using the Aerodyne Aerosol Chemical Speciation Monitor (ACSM), *Environ. Sci. Technol.*, 47, 5686–5694, 2013.
- Budisulistiorini, S. H., Canagaratna, M. R., Croteau, P. L., Baumann, K., Edgerton, E. S., Kollman, M. S., Ng, N. L., Verma, V., Shaw, S. L., Knipping, E. M., Worsnop, D. R., Jayne, J. T., Weber, R. J., and Surratt, J. D.: Intercomparison of an Aerosol Chemical Speciation Monitor (ACSM) with ambient fine aerosol measurements in downtown Atlanta, Georgia, *Atmos. Meas. Tech.*, 7, 1929–1941, doi:10.5194/amt-7-1929-2014, 2014.
- Canagaratna, M., Jayne, J., Jimenez, J. L., Allan, J. A., Alfarra, R., Zhang, Q., Onasch, T., Drewnick, F., Coe, H., Middlebrook, A., Delia, A., Williams, L., Trimborn, A., Northway, M., Kolb, C., Davidovits, P., and Worsnop, D.: Chemical and microphysical characterization of aerosols via Aerosol Mass Spectrometry, *Mass Spectrom. Rev.*, 26, 185–222, 2007.
- Cao, J., Xu, H., Xu, Q., Chen, B., and Kan, H.: Fine particulate matter constituents and cardiopulmonary mortality in a heavily polluted Chinese city, *Environ. Health Perspect.*, 120, 373–378, 2012.
- Carbone, S., Saarikoski, S., Frey, A., Reyes, F., Reyes, P., Castillo, M., Gramsch, E., Oyola, P., Jayne, J., and Worsnop, D. R.: Chemical characterization of submicron aerosol particles in Santiago de Chile, *Aerosol Air Qual. Res.*, 13, 462–473, 2013.
- Chen, Y., Sheng, G., Bi, X., Feng, Y., Mai, B., and Fu, J.: Emission factors for carbonaceous particles and polycyclic aromatic hydrocarbons from residential coal combustion in China, *Environ. Sci. Technol.*, 39, 1861–1867, doi:10.1021/es0493650, 2005.
- Cheng, Y., Engling, G., He, K.-B., Duan, F.-K., Du, Z.-Y., Ma, Y.-L., Liang, L.-L., Lu, Z.-F., Liu, J.-M., Zheng, M., and Weber, R. J.: The characteristics of Beijing aerosol during two distinct episodes: Impacts of biomass burning and fireworks, *Environ. Pollut.*, 185, 149–157, doi:10.1016/j.envpol.2013.10.037, 2014.
- DeCarlo, P. F., Kimmel, J. R., Trimborn, A., Northway, M. J., Jayne, J. T., Aiken, A. C., Gonin, M., Fuhrer, K., Horvath, T., Docherty, K. S., Worsnop, D. R., and Jimenez, J. L.: Field-Deployable, High-Resolution, Time-of-Flight Aerosol Mass Spectrometer, *Anal. Chem.*, 78, 8281–8289, 2006.
- Docherty, K. S., Aiken, A. C., Huffman, J. A., Ulbrich, I. M., DeCarlo, P. F., Sueper, D., Worsnop, D. R., Snyder, D. C., Peltier, R. E., Weber, R. J., Grover, B. D., Eatough, D. J., Williams, B. J., Goldstein, A. H., Ziemann, P. J., and Jimenez, J. L.: The 2005 Study of Organic Aerosols at Riverside (SOAR-1): instrumental intercomparisons and fine particle composition, *Atmos. Chem. Phys.*, 11, 12387–12420, doi:10.5194/acp-11-12387-2011, 2011.
- Draxler, R. R. and Rolph, G. D.: HYSPLIT (HYbrid Single-Particle Lagrangian Integrated Trajectory) Model access via NOAA ARL READY Website, <http://www.arl.noaa.gov/ready/hysplit4.html>, NOAA Air Resources Laboratory, Silver Spring, MD., 2003.
- Drewnick, F., Hings, S. S., DeCarlo, P. F., Jayne, J. T., Gonin, M., Fuhrer, K., Weimer, S., Jimenez, J. L., Demerjian, K. L., Borrmann, S., and Worsnop, D. R.: A new Time-of-Flight Aerosol Mass Spectrometer (ToF-AMS) – Instrument description and first field deployment., *Aerosol Sci. Technol.*, 39, 637–658, 2005.
- Gong, Z., Lan, Z., Xue, L., Zeng, L., He, L., and Huang, X.: Characterization of submicron aerosols in the urban outflow of the central Pearl River Delta region of China, *Front. Environ. Sci. Eng.*, 6, 725–733, doi:10.1007/s11783-012-0441-8, 2012.
- Guo, S., Hu, M., Zamora, M. L., Peng, J., Shang, D., Zheng, J., Du, Z., Wu, Z., Shao, M., Zeng, L., Molina, M. J., and Zhang, R.: Elucidating severe urban haze formation in China, *Proc. Natl. Acad. Sci. USA*, 111, 17373–17378, doi:10.1073/pnas.1419604111, 2014.
- Han, S., Kondo, Y., Oshima, N., Takegawa, N., Miyazaki, Y., Hu, M., Lin, P., Deng, Z., Zhao, Y., Sugimoto, N., and Wu, Y.: Temporal variations of elemental carbon in Beijing, *J. Geophys. Res.*, 114, D23202, doi:10.1029/2009JD012027, 2009.
- He, L.-Y., Huang, X.-F., Xue, L., Hu, M., Lin, Y., Zheng, J., Zhang, R., and Zhang, Y.-H.: Submicron aerosol analysis and organic source apportionment in an urban atmosphere in Pearl River Delta of China using high-resolution aerosol mass spectrometry, *J. Geophys. Res.*, 116, D12304, doi:10.1029/2010jd014566, 2011.
- Hu, M., Wu, Z., Slanina, J., Lin, P., Liu, S., and Zeng, L.: Acidic gases, ammonia and water-soluble ions in PM_{2.5} at a coastal site in the Pearl River Delta, China, *Atmos. Environ.*, 42, 6310–6320, doi:10.1016/j.atmosenv.2008.02.015, 2008.
- Hu, W. W., Hu, M., Yuan, B., Jimenez, J. L., Tang, Q., Peng, J. F., Hu, W., Shao, M., Wang, M., Zeng, L. M., Wu, Y. S., Gong, Z. H., Huang, X. F., and He, L. Y.: Insights on organic aerosol aging and the influence of coal combustion at a regional receptor site of central eastern China, *Atmos. Chem. Phys.*, 13, 10095–10112, doi:10.5194/acp-13-10095-2013, 2013.
- Huang, R.-J., Zhang, Y., Bozzetti, C., Ho, K.-F., Cao, J.-J., Han, Y., Daellenbach, K. R., Slowik, J. G., Platt, S. M., Canonaco, F., Zotter, P., Wolf, R., Pieber, S. M., Brun, E. A., Crippa, M., Ciarelli, G., Piazzalunga, A., Schwikowski, M., Abbaszade, G., Schnelle-Kreis, J., Zimmermann, R., An, Z., Szidat, S., Baltensperger, U., Haddad, I. E., and Prevot, A. S. H.: High secondary aerosol contribution to particulate pollution during haze events in China, *Nature*, 514, 218–222, doi:10.1038/nature13774, 2014.
- Huang, X.-F., He, L.-Y., Hu, M., Canagaratna, M. R., Sun, Y., Zhang, Q., Zhu, T., Xue, L., Zeng, L.-W., Liu, X.-G., Zhang, Y.-H., Jayne, J. T., Ng, N. L., and Worsnop, D. R.: Highly time-resolved chemical characterization of atmospheric submicron particles during 2008 Beijing Olympic Games using an Aerodyne High-Resolution Aerosol Mass Spectrometer, *Atmos. Chem. Phys.*, 10, 8933–8945, doi:10.5194/acp-10-8933-2010, 2010.
- Huang, X.-F., He, L.-Y., Hu, M., Canagaratna, M. R., Kroll, J. H., Ng, N. L., Zhang, Y.-H., Lin, Y., Xue, L., Sun, T.-L., Liu, X.-G., Shao, M., Jayne, J. T., and Worsnop, D. R.: Characterization of submicron aerosols at a rural site in Pearl River Delta of China using an Aerodyne High-Resolution Aerosol Mass Spectrometer, *Atmos. Chem. Phys.*, 11, 1865–1877, doi:10.5194/acp-11-1865-2011, 2011.
- Huang, X.-F., He, L.-Y., Xue, L., Sun, T.-L., Zeng, L.-W., Gong, Z.-H., Hu, M., and Zhu, T.: Highly time-resolved chemi-

- cal characterization of atmospheric fine particles during 2010 Shanghai World Expo, *Atmos. Chem. Phys.*, 12, 4897–4907, doi:10.5194/acp-12-4897-2012, 2012.
- Huang, X.-F., Xue, L., Tian, X.-D., Shao, W.-W., Sun, T.-L., Gong, Z.-H., Ju, W.-W., Jiang, B., Hu, M., and He, L.-Y.: Highly time-resolved carbonaceous aerosol characterization in Yangtze River Delta of China: composition, mixing state and secondary formation, *Atmos. Environ.*, 64, 200–207, doi:10.1016/j.atmosenv.2012.09.059, 2013.
- Huffman, J. A., Jayne, J. T., Drewnick, F., Aiken, A. C., Onasch, T., Worsnop, D. R., and Jimenez, J. L.: Design, modeling, optimization, and experimental tests of a particle beam width probe for the Aerodyne Aerosol Mass Spectrometer, *Aerosol Sci. Technol.*, 39, 1143–1163, 2005.
- Huffman, J. A., Docherty, K. S., Aiken, A. C., Cubison, M. J., Ulbrich, I. M., DeCarlo, P. F., Sueper, D., Jayne, J. T., Worsnop, D. R., Ziemann, P. J., and Jimenez, J. L.: Chemically-resolved aerosol volatility measurements from two megacity field studies, *Atmos. Chem. Phys.*, 9, 7161–7182, doi:10.5194/acp-9-7161-2009, 2009.
- Ianniello, A., Spataro, F., Esposito, G., Allegrini, I., Rantica, E., Ancora, M. P., Hu, M., and Zhu, T.: Occurrence of gas phase ammonia in the area of Beijing (China), *Atmos. Chem. Phys.*, 10, 9487–9503, doi:10.5194/acp-10-9487-2010, 2010.
- Jayne, J. T., Leard, D. C., Zhang, X., Davidovits, P., Smith, K. A., Kolb, C. E., and Worsnop, D. R.: Development of an aerosol mass spectrometer for size and composition analysis of submicron particles, *Aerosol Sci. Technol.*, 33, 49–70, 2000.
- Ji, D., Li, L., Wang, Y., Zhang, J., Cheng, M., Sun, Y., Liu, Z., Wang, L., Tang, G., Hu, B., Chao, N., Wen, T., and Miao, H.: The heaviest particulate air-pollution episodes occurred in northern China in January, 2013: Insights gained from observation, *Atmos. Environ.*, 92, 546–556, doi:10.1016/j.atmosenv.2014.04.048, 2014.
- Liu, Q.: Physical and chemical characteristics of submicron aerosol and its sources in Beijing, LAPC, Institute of Atmospheric Physics, Chinese Academy of Sciences, 2012.
- Matthew, B. M., Middlebrook, A. M., and Onasch, T. B.: Collection efficiencies in an Aerodyne Aerosol Mass Spectrometer as a function of particle phase for laboratory generated aerosols, *Aerosol Sci. Technol.*, 42, 884–898, 2008.
- Meng, Z. Y., Lin, W. L., Jiang, X. M., Yan, P., Wang, Y., Zhang, Y. M., Jia, X. F., and Yu, X. L.: Characteristics of atmospheric ammonia over Beijing, China, *Atmos. Chem. Phys.*, 11, 6139–6151, doi:10.5194/acp-11-6139-2011, 2011.
- Middlebrook, A. M., Bahreini, R., Jimenez, J. L., and Canagaratna, M. R.: Evaluation of composition-dependent collection efficiencies for the Aerodyne Aerosol Mass Spectrometer using field data, *Aerosol Sci. Technol.*, 46, 258–271, 2012.
- Ng, N. L., Herndon, S. C., Trimborn, A., Canagaratna, M. R., Croteau, P. L., Onasch, T. B., Sueper, D., Worsnop, D. R., Zhang, Q., Sun, Y. L., and Jayne, J. T.: An Aerosol Chemical Speciation Monitor (ACSM) for routine monitoring of the composition and mass concentrations of ambient aerosol, *Aerosol Sci. Technol.*, 45, 770–784, 2011.
- Parworth, C., Fast, J., Mei, F., Shippert, T., Sivaraman, C., Tilp, A., Watson, T., and Zhang, Q.: Long-term Measurements of Submicrometer Aerosol Chemistry at the Southern Great Plains (SGP) Using an Aerosol Chemical Speciation Monitor (ACSM), *Atmos. Environ.*, 106, 43–55, doi:10.1016/j.atmosenv.2015.01.060, 2015.
- Petit, J.-E., Favez, O., Sciare, J., Crenn, V., Sarda-Estève, R., Bonnaire, N., Mocnik, G., Dupont, J.-C., Haeffelin, M., and Leoz-Garziandia, E.: Two years of near real-time chemical composition of submicron aerosols in the region of Paris using an Aerosol Chemical Speciation Monitor (ACSM) and a multi-wavelength Aethalometer, *Atmos. Chem. Phys.*, 15, 2985–3005, doi:10.5194/acp-15-2985-2015, 2015.
- Polissar, A. V., Hopke, P. K., Paatero, P., Kaufman, Y. J., Hall, D. K., Bodhaine, B. A., Dutton, E. G., and Harris, J. M.: The aerosol at Barrow, Alaska: long-term trends and source locations, *Atmos. Environ.*, 33, 2441–2458, 1999.
- Sun, J., Zhang, Q., Canagaratna, M. R., Zhang, Y., Ng, N. L., Sun, Y., Jayne, J. T., Zhang, X., Zhang, X., and Worsnop, D. R.: Highly time- and size-resolved characterization of submicron aerosol particles in Beijing using an Aerodyne Aerosol Mass Spectrometer, *Atmos. Environ.*, 44, 131–140, 2010.
- Sun, Y. L., Wang, Z., Dong, H., Yang, T., Li, J., Pan, X., Chen, P., and Jayne, J. T.: Characterization of summer organic and inorganic aerosols in Beijing, China with an Aerosol Chemical Speciation Monitor, *Atmos. Environ.*, 51, 250–259, doi:10.1016/j.atmosenv.2012.01.013, 2012.
- Sun, Y. L., Wang, Z., Fu, P., Jiang, Q., Yang, T., Li, J., and Ge, X.: The impact of relative humidity on aerosol composition and evolution processes during wintertime in Beijing, China, *Atmos. Environ.*, 77, 927–934, doi:10.1016/j.atmosenv.2013.06.019, 2013a.
- Sun, Y. L., Wang, Z. F., Fu, P. Q., Yang, T., Jiang, Q., Dong, H. B., Li, J., and Jia, J. J.: Aerosol composition, sources and processes during wintertime in Beijing, China, *Atmos. Chem. Phys.*, 13, 4577–4592, doi:10.5194/acp-13-4577-2013, 2013b.
- Sun, Y. L., Jiang, Q., Wang, Z., Fu, P., Li, J., Yang, T., and Yin, Y.: Investigation of the sources and evolution processes of severe haze pollution in Beijing in January 2013, *J. Geophys. Res.*, 119, 4380–4398, doi:10.1002/2014JD021641, 2014.
- Viana, M., López, J. M., Querol, X., Alastuey, A., García-Gacio, D., Blanco-Heras, G., López-Mahía, P., Piñero-Iglesias, M., Sanz, M. J., Sanz, F., Chi, X., and Maenhaut, W.: Tracers and impact of open burning of rice straw residues on PM in Eastern Spain, *Atmos. Environ.*, 42, 1941–1957, doi:10.1016/j.atmosenv.2007.11.012, 2008.
- Wang, L. T., Wei, Z., Yang, J., Zhang, Y., Zhang, F. F., Su, J., Meng, C. C., and Zhang, Q.: The 2013 severe haze over southern Hebei, China: model evaluation, source apportionment, and policy implications, *Atmos. Chem. Phys.*, 14, 3151–3173, doi:10.5194/acp-14-3151-2014, 2014.
- Wang, S. X., Zhao, B., Cai, S. Y., Klimont, Z., Nielsen, C. P., Morikawa, T., Woo, J. H., Kim, Y., Fu, X., Xu, J. Y., Hao, J. M., and He, K. B.: Emission trends and mitigation options for air pollutants in East Asia, *Atmos. Chem. Phys.*, 14, 6571–6603, doi:10.5194/acp-14-6571-2014, 2014.
- Wang, Y., Zhang, Q. Q., He, K., Zhang, Q., and Chai, L.: Sulfate-nitrate-ammonium aerosols over China: response to 2000–2015 emission changes of sulfur dioxide, nitrogen oxides, and ammonia, *Atmos. Chem. Phys.*, 13, 2635–2652, doi:10.5194/acp-13-2635-2013, 2013.
- Wang, Z., Li, J., Wang, Z., Yang, W., Tang, X., Ge, B., Yan, P., Zhu, L., Chen, X., Chen, H., Wang, W., Li, J., Liu, B., Wang, X.,

- Wang, W., Zhao, Y., Lu, N., and Su, D.: Modeling study of regional severe hazes over mid-eastern China in January 2013 and its implications on pollution prevention and control, *Sci. China Earth Sci.*, 57, 3–13, doi:10.1007/s11430-013-4793-0, 2014.
- Xu, J., Zhang, Q., Chen, M., Ge, X., Ren, J., and Qin, D.: Chemical composition, sources, and processes of urban aerosols during summertime in northwest China: insights from high-resolution aerosol mass spectrometry, *Atmos. Chem. Phys.*, 14, 12593–12611, doi:10.5194/acp-14-12593-2014, 2014.
- Xu, W. Y., Zhao, C. S., Ran, L., Lin, W. L., Yan, P., and Xu, X. B.: SO₂ noontime-peak phenomenon in the North China Plain, *Atmos. Chem. Phys.*, 14, 7757–7768, doi:10.5194/acp-14-7757-2014, 2014.
- Yang, F., Huang, L., Duan, F., Zhang, W., He, K., Ma, Y., Brook, J. R., Tan, J., Zhao, Q., and Cheng, Y.: Carbonaceous species in PM_{2.5} at a pair of rural/urban sites in Beijing, 2005–2008, *Atmos. Chem. Phys.*, 11, 7893–7903, doi:10.5194/acp-11-7893-2011, 2011.
- Zhang, H., Wang, S., Hao, J., Wan, L., Jiang, J., Zhang, M., Mestl, H. E. S., Alnes, L. W. H., Aunan, K., and Mellouki, A. W.: Chemical and size characterization of particles emitted from the burning of coal and wood in rural households in Guizhou, China, *Atmos. Environ.*, 51, 94–99, doi:10.1016/j.atmosenv.2012.01.042, 2012.
- Zhang, Q., Jimenez, J. L., Worsnop, D. R., and Canagaratna, M.: A case study of urban particle acidity and its effect on secondary organic aerosol, *Environ. Sci. Technol.*, 41, 3213–3219, 2007.
- Zhang, R., Jing, J., Tao, J., Hsu, S. C., Wang, G., Cao, J., Lee, C. S. L., Zhu, L., Chen, Z., Zhao, Y., and Shen, Z.: Chemical characterization and source apportionment of PM_{2.5} in Beijing: seasonal perspective, *Atmos. Chem. Phys.*, 13, 7053–7074, doi:10.5194/acp-13-7053-2013, 2013.
- Zhang, Y., Schauer, J. J., Zhang, Y., Zeng, L., Wei, Y., Liu, Y., and Shao, M.: Characteristics of particulate carbon emissions from real-world Chinese coal combustion, *Environ. Sci. Technol.*, 42, 5068–5073, 2008.
- Zhang, Y., Sun, J., Zhang, X., Shen, X., Wang, T., and Qin, M.: Seasonal characterization of components and size distributions for submicron aerosols in Beijing, *Sci. China Earth Sci.*, 56, 890–900, doi:10.1007/s11430-012-4515-z, 2013.
- Zhang, Y. J., Tang, L. L., Wang, Z., Yu, H. X., Sun, Y. L., Liu, D., Qin, W., Canonaco, F., Prévôt, A. S. H., Zhang, H. L., and Zhou, H. C.: Insights into characteristics, sources, and evolution of submicron aerosols during harvest seasons in the Yangtze River delta region, China, *Atmos. Chem. Phys.*, 15, 1331–1349, doi:10.5194/acp-15-1331-2015, 2015.
- Zhao, P. S., Dong, F., He, D., Zhao, X. J., Zhang, X. L., Zhang, W. Z., Yao, Q., and Liu, H. Y.: Characteristics of concentrations and chemical compositions for PM_{2.5} in the region of Beijing, Tianjin, and Hebei, China, *Atmos. Chem. Phys.*, 13, 4631–4644, doi:10.5194/acp-13-4631-2013, 2013.
- Zhao, X., Zhang, X., Xu, X., Xu, J., Meng, W., and Pu, W.: Seasonal and diurnal variations of ambient PM_{2.5} concentration in urban and rural environments in Beijing, *Atmos. Environ.*, 43, 2893–2900, 2009.
- Zheng, G. J., Duan, F. K., Su, H., Ma, Y. L., Cheng, Y., Zheng, B., Zhang, Q., Huang, T., Kimoto, T., Chang, D., Pöschl, U., Cheng, Y. F., and He, K. B.: Exploring the severe winter haze in Beijing: the impact of synoptic weather, regional transport and heterogeneous reactions, *Atmos. Chem. Phys.*, 15, 2969–2983, doi:10.5194/acp-15-2969-2015, 2015.
- Zheng, M., Salmon, L. G., Schauer, J. J., Zeng, L., Kiang, C. S., Zhang, Y., and Cass, G. R.: Seasonal trends in PM_{2.5} source contributions in Beijing, China, *Atmos. Environ.*, 39, 3967–3976, doi:10.1016/j.atmosenv.2005.03.036, 2005.